Optical Engineering

OpticalEngineering.SPIEDigitalLibrary.org

# Compact laser radar based on a subnanosecond laser diode transmitter and a two-dimensional CMOS single-photon receiver

Jaakko Huikari
Sahba Jahromi
Jussi-Pekka Jansson
Juha Kostamovaara

SPIE.

Jaakko Huikari, Sahba Jahromi, Jussi-Pekka Jansson, Juha Kostamovaara, "Compact laser radar based on a subnanosecond laser diode transmitter and a two-dimensional CMOS single-photon receiver," *Opt. Eng.* **57**(2), 024104 (2018), doi: 10.1117/1.OE.57.2.024104.

Optical Engineering 57(2), 024104 (February 2018)

# Compact laser radar based on a subnanosecond laser diode transmitter and a two-dimensional CMOS single-photon receiver

**Jaakko Huikari,* Sahba Jahromi, Jussi-Pekka Jansson, and Juha Kostamovaara**
University of Oulu, Faculty of Information Technology and Electrical Engineering, Circuits and Systems Research Group, Oulu, Finland

**Abstract.** A pulsed TOF laser radar utilizing the single-photon detection mode has been implemented, and its performance is characterized. The transmitter employs a QW double-heterostructure laser diode producing 0.6 nJ/100 ps laser pulses at a central wavelength of ~810 nm. The detector is a single-chip IC manufactured in the standard 0.35-$\mu$m HV CMOS process, including a $9 \times 9$ single-photon avalanche diode (SPAD) array and a 10-channel time-to-digital converter (TDC) circuit. Both the SPAD array and the TDC circuit support a time gating feature allowing photon detection to occur only within a predefined time window. The SPAD array also supports a $3 \times 3$ SPADs subarray selection feature to respond to the laser spot wandering effect due to the paraxial optics and to reduce background radiation-induced detections. The characterization results demonstrate a distance measurement accuracy of $+/-0.5$ mm to a target at 34 m having 11% reflectivity. The signal detection rate is 28% at a laser pulsing rate of 100 kHz. The single-shot precision of the laser radar is ~20 mm (FWHM). The deteriorating impact of high-level background radiation conditions on the SNR is demonstrated, as also is a scheme to improve this by means of detector time gating.  [DOI: 10.1117/1.OE.57.2.024104]

Keywords: laser ranging; pulsed time-of-flight laser radar; single-photon avalanche diode array; subnanosecond laser pulse; time gating; miniature module.

Paper 171854 received Nov. 20, 2017; accepted for publication Jan. 30, 2018; published online Feb. 19, 2018.

## 1 Introduction

Time-of-flight (TOF) laser radar techniques have been widely used for distance measurement applications such as the measurement of material levels in containers, profiling and scanning of objects, traffic safety applications such as collision avoidance, speed measurement, and traffic control, and positioning, surveying, and docking. One important advantage of optical radars over microwave radars, for example, is easy collimation of the optical beam with lenses. Due to the much shorter wavelength, the diffraction-limited spot size $\phi_{\mathrm{div}} \sim \lambda/D$ is also much smaller, and thus the spatial resolution of the measurement can be high, typically only a few millimeters or centimeters.[1–4]

Optical radars typically use either pulsed TOF or phase comparison techniques based on a continuous wave (CW) laser source.[5] Both techniques have been used successfully in a wide variety of applications. It is the pulsed TOF principle that is used here. In this technique, the transit time of a short laser pulse from the transmitter to the object and then back to the receiver is measured with a time-to-digital converter (event detection-based timing), and the target distance is calculated from this based on the known speed of light. The main advantage of this approach over CW-based techniques is that high precision can be achieved even with a single laser shot.[3]

The block diagram of a pulsed TOF laser radar system is shown in Fig. 1. Typically, a pulsed TOF laser radar uses either a PIN or an avalanche photo diode (APD) as the photodetector and the receiver works in the linear operation mode, i.e., it produces a voltage signal that is in principle proportional to the current pulse of the photodetector (and thus to the envelope of the optical echo). The electrical receiver noise is in this case the key parameter limiting the sensitivity of the radar. Thus, a wideband receiver with low noise and a wide linear operation range is needed, which poses a serious challenge when designing pulsed TOF laser radars of this kind.[6]

In this work, we employ single-photon techniques for the detection of the optical echo rather than the well-established linear receiving techniques.[7,8] Moreover, the single-photon detector is realized as a two-dimensional (2-D) array in a standard CMOS technology. A single-photon avalanche diode (SPAD) is a $p-n$ junction reverse-biased above its breakdown voltage. At this operation point, a photon that is absorbed into the depletion region may cause a rapidly accumulating avalanche breakdown, resulting in a digital timing signal with a ~50- to 100-ps jitter.[9,10] No separate analog receiver (including, e.g., low-noise preamplifier and postamplifiers) is needed, and thus the receiver complexity can be markedly reduced even with improved sensitivity. Since the single-shot precision is now determined by the laser pulse width as a first-order approximation, this width is also reduced from the value of 3 to 4 ns (FWHM), which is typically used in pulsed TOF laser radars to ~100 ps. This pulse is produced at a relatively high-energy level (~0.6 nJ), with a specially designed quantum well double heterostructure (QW DH) laser diode with enhanced gain switching.[11,12]

*Address all correspondence to: Jaakko Huikari, E-mail: jaakko.huikari@oulu.fi

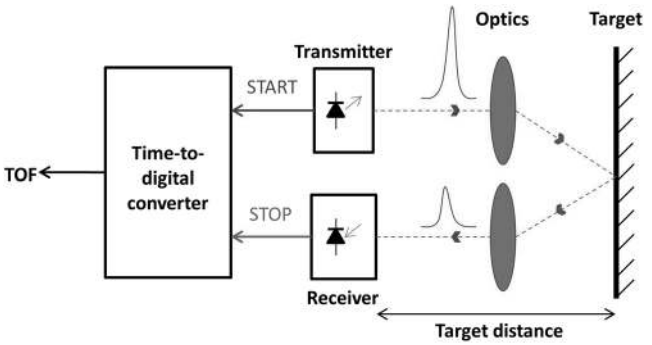


**Fig. 1** A pulsed TOF laser radar system.

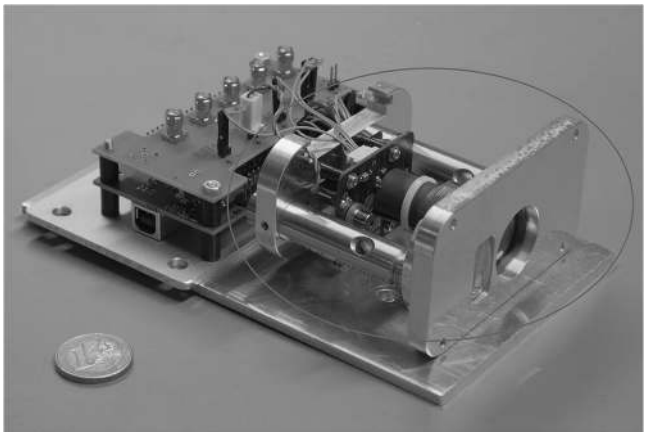

**Fig. 2** Miniature laser radar.

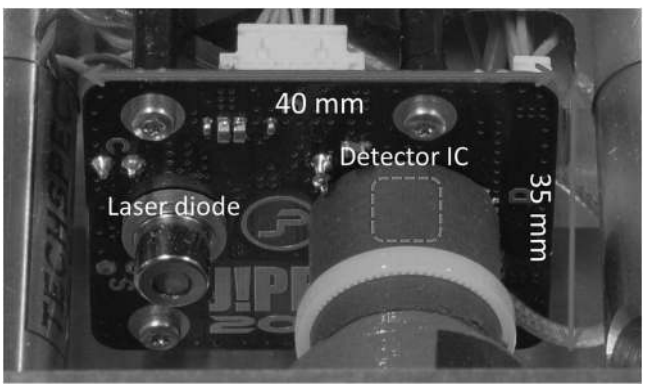


**Fig. 3** Transmitter–receiver PCB.

The electronics of the whole laser radar, including the transmitter and receiver, are constructed on a single printed circuit board (PCB). As pointed out above, the single-photon detector is realized as a 2-D detector array that is larger in area than the receiver spot size. The detector array can be electrically configured so that the received optical signal is detected only by those detector elements that are actually exposed to the received optical echo. This construction allows a large detector area without increasing the noise produced by the background radiation, which is proportional to the field of view (FOV) of the detector element. The large area is important since it allows the received laser spot image to move within the detector area, which inevitably happens with biaxial optics. The large area and electrical configurability of the detector can also be utilized in minimizing the timing walk error, by acquiring TOF information only from those SPAD elements operating in the single-photon mode. In addition, this construction reduces the accuracy of the tolerances in the mechanical adjustments of the laser radar system.

Single-photon detection techniques have been intensively studied and applied for pulsed TOF range finding and the scanning of distant objects. Implementations vary from 1-D to 3-D scanning based on either 1-D measurement data or on a flash-type scanner illuminating the whole 3-D scene, see e.g., [13–17] and references therein. Thus, the basic properties of single-photon detection techniques are well known. On the other hand, compact laser transmitters with high power and sub-ns pulses are not readily available. Low probe pulse power cannot be straight-forwardly compensated for using a higher pulsing rate, since this would also increase the total number of background photon detections and thus reduce the signal-to-noise ratio under high background illumination conditions.

The paper proceeds as follows: after the introduction chapter in Sec. 1, the implementation of the 1-D pulsed TOF laser radar system is described in Sec. 2. The measurements characterizing the performance of the radar are given in Sec. 3. Two feasibility studies are described, and their results are presented and discussed in Sec. 4, and finally, the discussion and conclusions are given in Sec. 5.

## 2 Implementation

### 2.1 *General Architecture*

The architecture of the proposed pulsed time-of-flight laser radar using single photon detection techniques follows the block diagram of Fig. 1,[18] whereas Fig. 2 shows a photograph of the full laser radar laboratory setup, in which the transmitter–receiver module is indicated by a circle.

The transmitter and receiver electronics are implemented on a single PCB of size 3.5 cm × 4.0 cm, with a distance of ∼20 mm between the laser diode and the detector IC. The transmitter consists of a laser diode capable of producing high-power (∼5 W) and high-speed (FWHM ∼100 ps) laser pulses using a relatively simple pulsing scheme realized with a high-speed MOS switch driving an RLC circuit.[19]

The receiver, including a 2-D 9 × 9 SPAD array detector and a 10-channel time-to-digital converter (TDC) circuit, is a single-chip IC manufactured in a standard 0.35-$\mu$m high-voltage complementary metal-oxide semiconductor (HV CMOS) process having total chip dimensions of 2.5 mm × 4 mm.[20] The photograph in Fig. 3 shows the dimensions of the transmitter–receiver PCB and the locations of the laser diode and receiver IC, the outline of which is denoted by the dash line on the stray light cover.

### 2.2 *Transmitter*

The laser pulse transmitter, a schematic diagram of which is shown in Fig. 4, uses a customized QW double-heterostructure laser diode with an active stripe width of 30 $\mu$m and a cavity length of 3.0 mm. The center wavelength of the laser emission is ∼810 nm. The laser diode operates in the enhanced gain-switching mode, which is achieved using a large equivalent spot size $d_a/\Gamma_a$ (thickness of the active

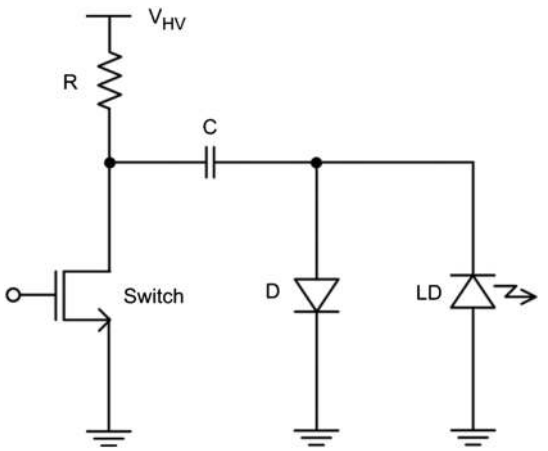


**Fig. 4** Schematic diagram of a laser pulse transmitter.

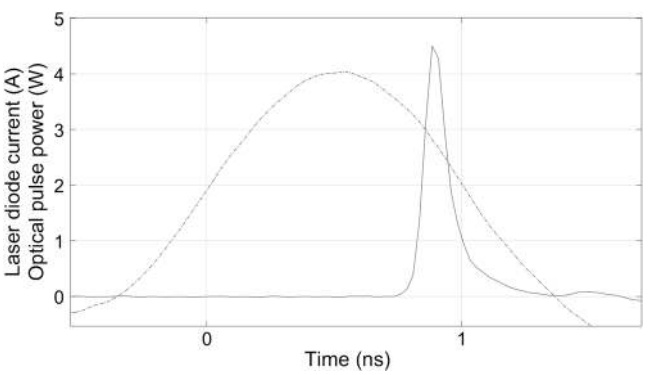


**Fig. 5** The drive current pulse and laser pulse of the laser diode.

area/optical confinement factor) in its construction.[11] As a result, it is capable of producing sub-ns pulses (FWHM ~100 ps) at a relatively high-power level (~5 W). Thus, the pulse energy is ~0.6 nJ, which is considerably greater than that available in the standard gain-switching regime.[21,22] The current pulse needed to drive the laser diode to produce this optical pulse has an amplitude of 4 A and a pulse width of 1 ns (FWHM). It is important to note that even though the drive current has a width of ~1 ns, the laser diode itself produces an optical output with a width of 100 ps as a result of its internal operation. The transmitter electronics also produce the start pulse for the time interval measurement circuit, marking the time stamp of the moment of the laser pulse emission. The current pulse and the corresponding optical pulse shapes, the dash line and the solid line, respectively, measured with a bandwidth of 12 GHz, are shown in Fig. 5. The pulsing frequency of the laser diode was set to 100 kHz.

### 2.3 *2-D CMOS Single-Photon Avalanche Diode Array*

A picture of the receiver IC layout is shown in Fig. 6. The total dimensions of the SPAD array are 330 $\mu$m × 330 $\mu$m, whereas the detector array includes 9 × 9 SPADs. Any of the available 49 subarrays, with 3 × 3 SPAD elements in each, can be selected electrically and connected to the nine separate TCD channels to act as stop signals for the TOF

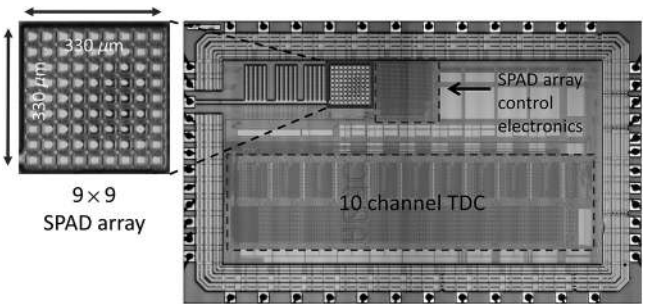


**Fig. 6** The receiver IC layout.

measurement. This feature allows tracking of the laser spot on the image plane while keeping the subarray FOV small, thus reducing background photon-induced noise.

Since the stripe width of the laser diode is 30 $\mu$m and the transmitter and receiver optics have equal focal lengths, the field of view of the whole SPAD array is larger than that of the laser diode by a factor of 10. This allows the received echo images to wander on the detector surface and also relaxes the accuracy needed in the optomechanical adjustments. The 24 $\mu$m × 24 $\mu$m size of a single SPAD element is proportional to the laser stripe width.[20]

The fill factor of the SPAD array (active area/total area) is around 50%, and the photon detection efficiency of a single SPAD element is ~4% at a wavelength of 810 nm. The typical timing jitter is of the order of ~80 ps, which corresponds well to the laser pulse width, resulting in a single-shot precision of the order of 100 to 150 ps for the system as a whole.[7,20]

All the SPAD elements share common quench and load signals but their enable signals are separate and determine which of the SPAD elements are activated for photon detection. Each SPAD element also has a self-quench mechanism to bring the photon detection-induced breakdown current to zero after a photon detection incident. In addition, the SPAD elements selected can be set in the photon detection mode at a desired point in time after laser pulse generation with a time resolution of ~4 ns. This feature, called time gating, helps to avoid blocking of the receiver for distant targets under high background illumination conditions.[7]

### 2.4 *Time Interval Measurement Circuit*

The receiver IC also contains a 10-channel TDC circuit, a more detailed description of which is given in Ref. 23. The operating principle of the TDC is based on a counter and two interpolators, and its purpose is to measure the time intervals between the start signal generated by a laser drive current pulse and the nine separate stop signals induced by SPAD triggering. The maximum time range which the TDC is capable of measuring is ~533 ns (equivalent to ~80 m in distance), with a single-shot precision of 10 ps ($\sigma$ value). The TDC also supports the time gating feature, allowing the stop signal to be recorded only after a certain time interval following the start signal. The measured TOF time interval data, 18 bytes per measurement, are transmitted to a PC by an FPGA board, which also handles the detector IC configuration at the beginning of TOF measurement.[23,24]

### 2.5 *Optics*

Both the transmitter and the receiver employ achromatic lenses with a focal length of 40 mm and diameter of 20 mm. The transmitter lens width was cut to 9 mm in 1-D to reduce the distance between the transmitter and the receiver. The receiver's optical path includes a bandpass filter, a center wavelength of 800 nm, and a bandwidth of 50 nm, to reduce detections induced by background radiation, i.e., noise. The transmitter beam divergence is 0.75 mrad and that of the receiver, defined by the whole $9 \times 9$ SPAD array area, is 8.25 mrad. The divergence for an individual SPAD element is ~0.75 mrad.

## 3 Measurements and Results

System characterization measurements were carried out to define the walk error, linearity, signal detection rate, single-shot precision, and target distance-dependent behavior of the laser spot image on the surface of the SPAD array. The TOF measurement data were accumulated with 18 target distances varying from 1 to 34 m. The measurements were performed using a calibrated and automated linearity measurement track with an estimated target location accuracy of $+/-0.3$ mm. The total number of laser pulses applied per unit of measurement distance was 560,000. The detector gate window was opened ~25 ns before the target, and the reflectance of the target was ~11%. The subarray selection was done before the individual measurement sequence. The location of the reflected laser spot image on the detector surface at each target distance was found by scanning detections throughout the whole $9 \times 9$ SPAD array. The background radiation level during the measurements was <50 lx (normal laboratory conditions). The laser radar was located at a minus offset of ~45 cm from the origin of the linearity measurement track.

Walk error measurements were performed to quantify how the distance measurement systematically depends on the power level of the received signal. The higher the received signal level, i.e., the more photons the SPAD detector absorbs, the faster the avalanche builds up, and, consequently, the shorter the TOF and the closer the target appears to be to the distance measurement system. The less energetic phenomena, spontaneous emission and super luminescence taking place before the onset of the rising edge of the laser pulse, also become visible to the receiver at higher received signal levels. The optical power reflected from the target to the receiver is dependent on the surface material of the target, the reflection coefficient of natural surfaces typically varying between 0.1 and 1. Three target reflectivity values were used here to alter the level of the received signal. The target materials used and their reflectivity values were: black rubber (4%), white copy paper (~100%), and a highly directional diamond grade reflector (≫100%). The target distance for the walk error measurements was 14 m.

Finally, photodetector time gating measurements were performed under conditions of high background radiation levels, the signal detection rate being recorded as a function of the length of the time interval from the enabling of the SPAD array to detection of the photons reflected from the target. Detector time gating can be applied to improve the photodetector's ability to see the signal photons reflected from the target under conditions of high background radiation. The measurement was performed outdoors around noon

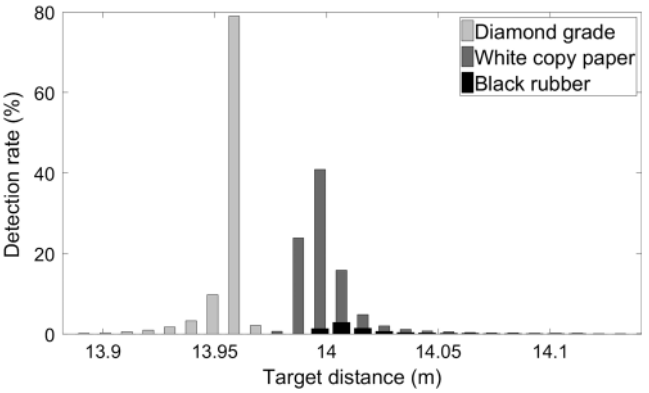


**Fig. 7** Walk error.

to maximize the background radiation level. The sky was clear, and the measured background radiation was ~90 klx. Ten gate opening times were tested, from 7.7 to 220 ns. The target was at a distance of 34 m and its reflectance coefficient was ~16%. Another similar detector time gating measurement was performed when the target distance was 73.2 m, i.e., virtually at the limit imposed on the laser radar by the TDC circuit, thus constituting the ultimate test of its performance. In this case, only the two extreme gate widths were used.

### 3.1 *Walk Error*

The three TOF histograms in Fig. 7 apply to a single SPAD with the highest signal detection rate. The location of the histogram of the single shot time intervals shifts in the direction of earlier timing as the reflected signal power increases. For example, the shift between the black rubber and diamond-grade reflectors, i.e., the timing walk error, is ~5 cm. In the case of the black rubber target, the received power is low and the avalanche breakdowns are due to single detected photons, and since the detector SPAD is operating in the single photon mode, walk error-free distance measurements are produced. In the case of the diamond-grade reflector, the avalanche breakdowns are due to a large quantity of photons, which leads to more rapidly accumulating avalanche breakdowns, thus causing timing walk error. The detections from the white paper target reflections are also multiphoton in nature but weaker in scale.

### 3.2 *Linearity*

Linearity error has been defined as the deviation of the average of the TOF results achieved from the nine SPADs from a reference line fitted by the method of least squares. Here, the difference between the two linearity error curves in Fig. 8 is due to the distinct data processing methods employed. In the first method, the lower solid line curve, the TOF result for every SPAD was calculated from its histogram as the mean of the TOF values of the peak bin and its four neighbor bins, two bins on each side (peak region-weighted TOF value). The average value (final TOF result) was then calculated as the weighted average of the nine separate TOF results, each being weighted by the corresponding detection rate of the SPAD. In the second method, the dash line curve, no SPADwise detection rate weighting was used. In addition, the reference line for the dash line curve was based on the

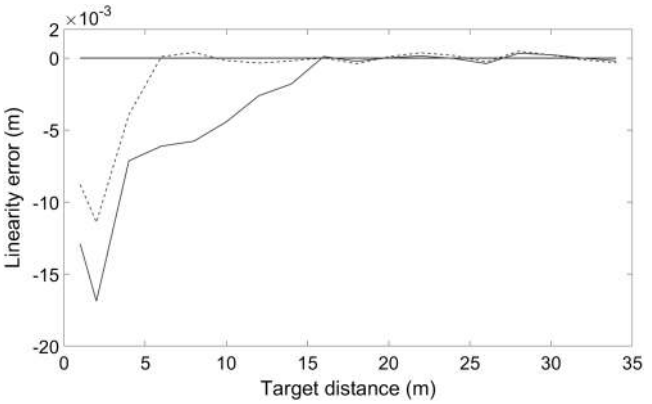


**Fig. 8** Linearity error versus target distance.

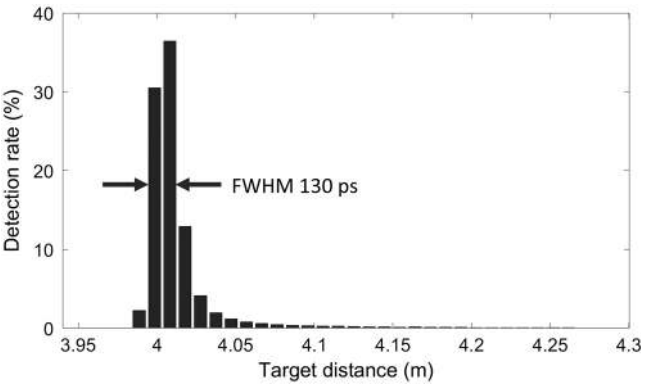


**Fig. 10** Detection rate with the target at 4 m.

average of the nine peak region-weighted TOF values from 6 to 34 m, whereas the values for the solid line curve ranged from 16 to 34 m. The measured linearity in both cases was $+/-0.5$ mm within the above ranges. The total number of laser pulses applied per unit of measurement distance was 560,000.

At target distances of 16 m and above the curves do indeed coincide, due to the low received optical power. At this power level, the SPAD elements operate in the single photon mode and the distance measurement is walk error-free. In contrast, at target distances below 16 m the curves deviate, since the received power level is higher, leading the SPADs eventually into the multiphoton mode, which will introduce walk error. Note, however, that since the energy distribution within the image spot on the detector surface is not even, the SPADs near the edge of the spot receive less energy, which causes a smaller walk error in their results. Thus, the results achieved with SPADs working in the single-photon detection mode should obviously be used only to produce the final result, since this leads to the lowest walk error, as indicated by the results given here. The kink between the results for one and two meters is due to the laser spot finally wandering partially off the SPAD array, thus reducing the received optical power and the resulting walk error.

### 3.3 *Detection Rate*

In Fig. 9, the solid line shows the combined measurement rate of the nine SPAD elements (max value 900%) curve and the dash line a reference curve for the detection rate based on the theoretical radar Eq. (1) as a function of the target distance

$$P(Z) = \frac{A_r}{\pi \cdot Z^2} \cdot P_0 \cdot \tau \cdot \epsilon \cdot \mathrm{PDP} \cdot FF \cdot A_f. \quad (1)$$

The radar equation parameters employed here are transmitted pulse energy $P_0$ of 0.6 nJ, an optic efficiency $\tau$ of 80%, an aperture area $A_r$ of $3.14 \cdot 10^{-4}$ m$^2$, and a target reflectivity $\epsilon$ of 11%. The other, less certain parameters and their values are an SPAD array fill factor $FF \sim 50\%$, a photon detection efficiency PDP of 4% and a receiver optical bandpass filter efficiency $A_f$ of 75%. The variable $Z$ is the target distance.[25]

The curves do coincide closely at target distances above ~20 m, where the received optical power is relatively low and the combined detection rate is below 100%. Most of the SPAD elements are then in the single-photon mode and the detector is in the linear operation mode. The spot size is small and most of the spot energy is received by one or two SPAD elements.

In the distance range of $< \sim 20$ m, however, the curves do deviate from each other. Higher received power and increased spot size result in a situation, where more SPADs are operating in a multiphoton mode, i.e., in saturation, which is reflected in saturation of the detection rate as well. The steep collapse of the detection rate at target distances of <4 m is caused by the spot finally wandering outside the detector array. Also, the spot size becomes larger than the subarray, due to defocusing of the optics, and thus only a fraction of the spot energy is falls onto it.

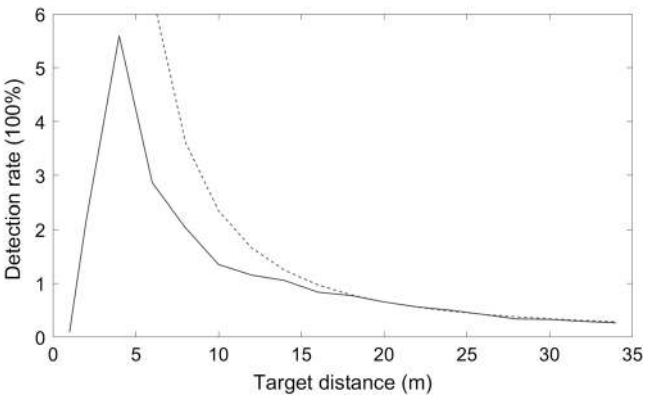


**Fig. 9** Detection rate versus target distance.

### 3.4 *Single-Shot Precision*

Two single-shot time interval histograms of a single SPAD with the highest detection rate at two target distances, 4 and 34 m, are shown in Figs. 10 and 11. The FWHM of the histograms, based on a TDC bin width of 65 ps, is 130 ps, corresponding to a distance measurement single-shot precision of ~2 cm. The signal detection rates were 95% and 10%, respectively.

### 3.5 *Laser Spot Image on a Single-Photon Avalanche Diode Array*

A series of 3-D sketches in Fig. 12, representing the energy distributions of a laser spot image on a $9 \times 9$ SPAD array, illustrates the size of the spot image and its location on

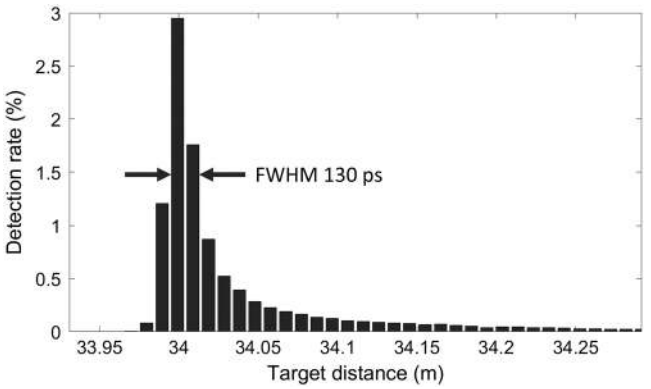


**Fig. 11** Detection rate with the target at 34 m.

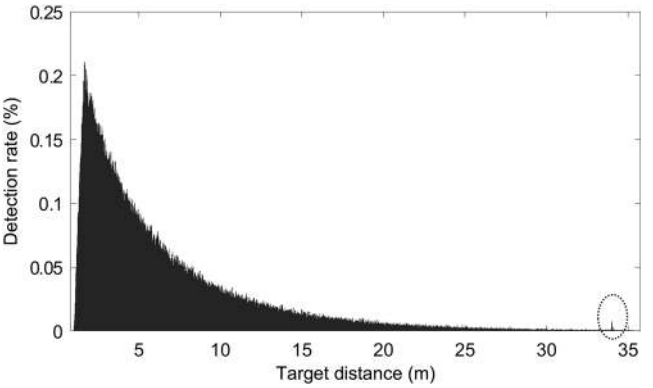


**Fig. 13** Detection rate with the target at 34 m and a wide time gate.

the SPAD array at six target distances. The *Y*-axis represents the signal detection rate value. The spot size is largest at distances of 2 and 4 m, (b) and (c), respectively, and its location has shifted to the left, i.e., away from the transmitter (note the different *Y*-axis scales). An increase in the spot size is due to defocusing of the optics and the spot shift due to a geometric shift caused by the paraxial optics used.

### 3.6 *Detector Behavior under High-Level Background Radiation Conditions*

A histogram of single shots in a single SPAD (receiving most of the signal energy) measured with a very wide time gate of ~200 ns under high background illumination conditions (90 klx, bright sunlight) is shown in Fig. 13. The target is located at 34 m and its reflection coefficient is 16%. As is seen, most of the recorded detections are produced by the background radiation and the target is almost completely blocked, since only ~0.02% of the laser shots result in the valid detection of any signal photons reflected from the target. The mean time between background-induced detections can be calculated from the exponential decay to be ~35 ns. As an example, the TOF histogram in Fig. 14 illustrates the signal detection rate of a single SPAD receiving most of the reflected energy with a narrow time gate window of ~12 ns.

The reduction in the signal detection rate caused by background radiation detections can be ameliorated by time gating the SPADs to the detection mode only just before the probe photons reflected from the target arrive at the

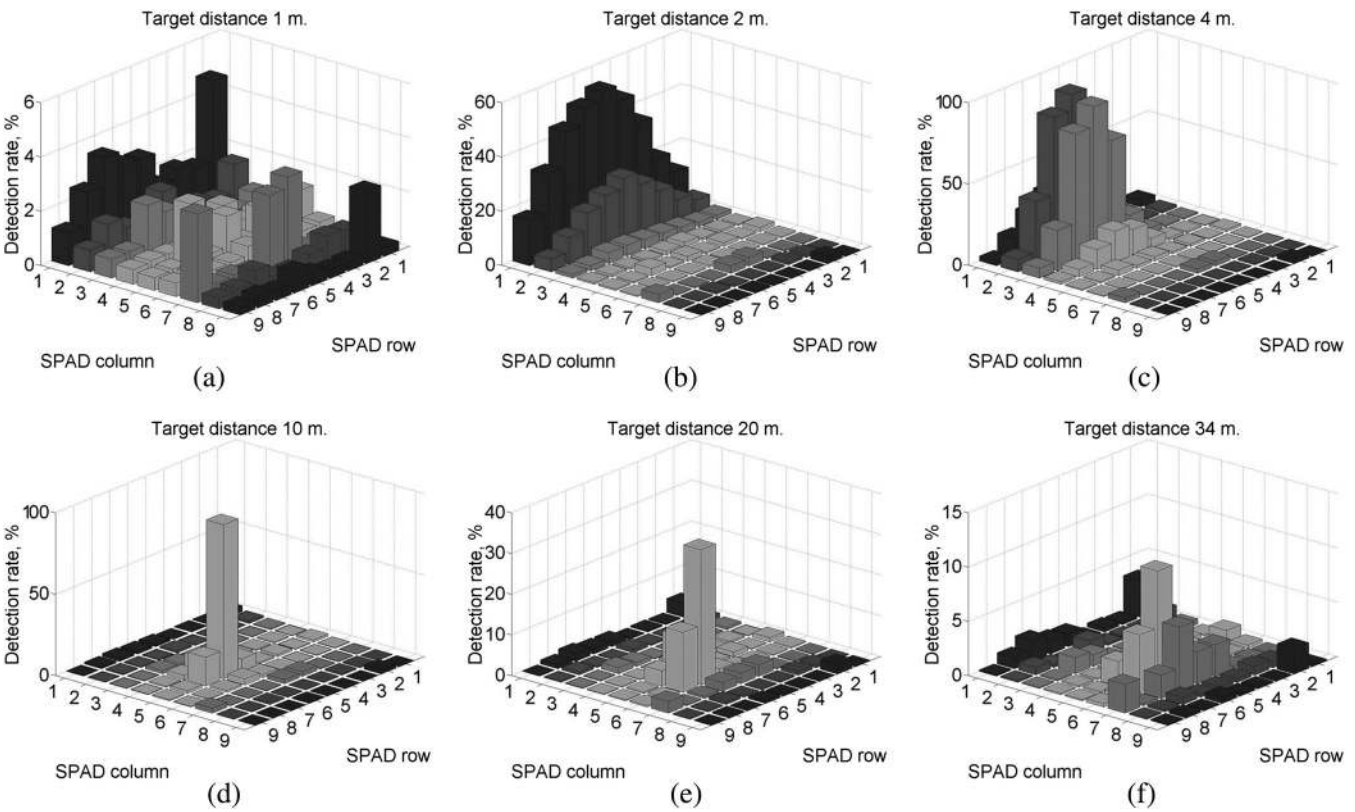


**Fig. 12** Energy distribution of a laser spot image on a SPAD array at six target distances: (a) 1 m, (b) 2 m, (c) 4 m, (d) 10 m, (e) 20 m, and (f) 34 m.

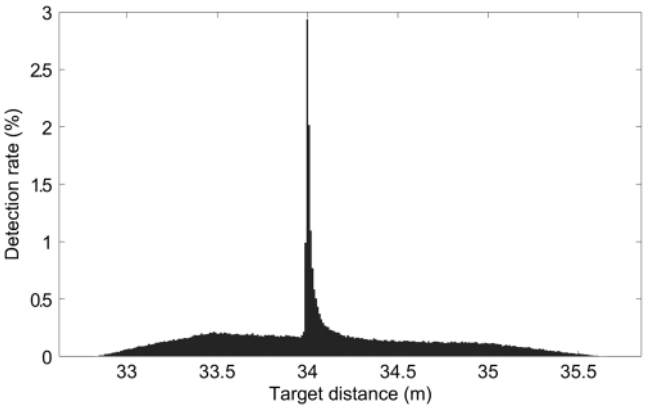


**Fig. 14** Detection rate with the target at 34 m and a narrow time gate.

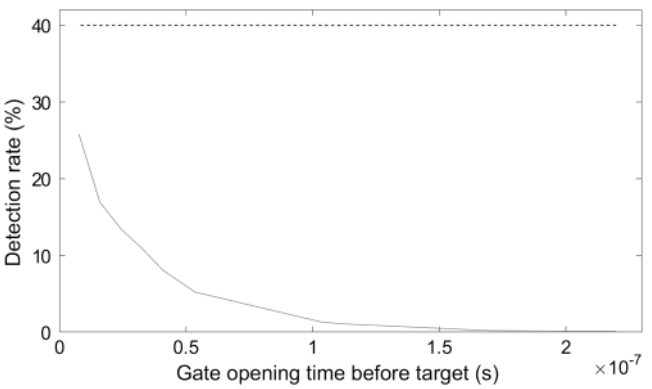


**Fig. 15** Combined signal detection rate versus total gate opening time.

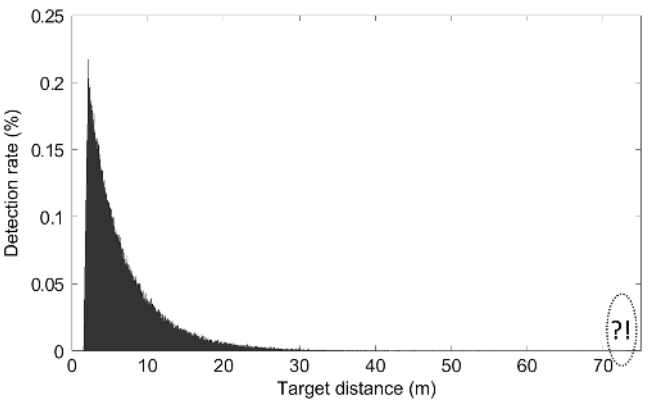


**Fig. 16** Detection rate with the target at 73.2 m and a wide time gate. Note the total absence of detections from the target.

detector. A curve for the combined signal detection rate (calculated from all nine SPADs) versus total gate window opening time before the arrival of the signal photons from the target is shown in Fig. 15. The dash line is the reference signal detection rate, ~40%, which was measured under conditions of low-level background radiation to be <50 lx. The signal detection curve shows, for example, that when the SPADs are gated to 50 ns before the signal photons arrival, the total signal detection rate is ~5%, whereas if the SPADs are gated to 25 ns, the total signal detection

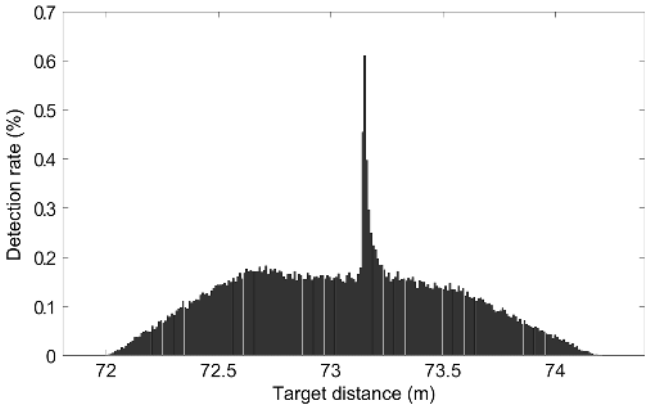


**Fig. 17** Detection rate, the target at 73.2 m and a narrow time gate.

rate increases to ~13%. The histograms in Figs. 16 and 17 show corresponding wide and narrow time gate measurements for a target at a distance of ~73 m.

Thus detector time gating can be effectively used to avoid background photon blocking of the detector in single photon detection-based laser ranging. On the other hand, with high-level background illumination, the signal-to-noise ratio (SNR) will still be limited by the background detections, so that intensive averaging of successive measurements is needed. For example, given the results in Figs. 13 and 14, the probability of background detection in the first measurement channels will be around 0.2% (~65 ps/34 ns). If the signal detection rate were at the same level, a few thousand laser shots would be needed to get a detectable signal included in the histogram of the results (~10,000 shots for a SNR of ~5).

## 4 Feasibility Studies

Two feasibility studies were performed to demonstrate the submillimeter distance measurement precision and centimeter-level spatial resolution achievable with the relatively high-energy sub-ns laser pulse with low divergence used in the 1-D laser radar implemented here. In the first study, the 1-D radar was used to measure a person's breathing pattern. The test person was located ~4 m from the radar with his back against the wall to minimize longitudinal motion of the target other than that involved in breathing. The laser spot was directed to the naked skin immediately below the sternum. The probe signal pulsing frequency was 100 kHz. The individual breathing pattern curve points in Fig. 18 were acquired by averaging 1000 successive measurements thus providing distance measurement results with submillimeter precision. The measurement data were then filtered by the moving-average method using window size of 15 to reduce noise in the breathing pattern curve. Note two deep breathing sections and a breath-holding section in between them (roughly from 33 to 48 s). During each deep breathing section, a frequency of ~1/7 Hz and max amplitude of ~1.2 cm can be observed in the curve, whereas the magnified presentation of the breath-holding section in Fig. 19 shows minuscule kinks along the curve that are with a frequency of around 1 to 2 Hz and an amplitude of <1 mm, which are due to heart contractions.[26] The detection rate during the measurement was ~100% due to the short target distance and the high reflectivity of the skin.

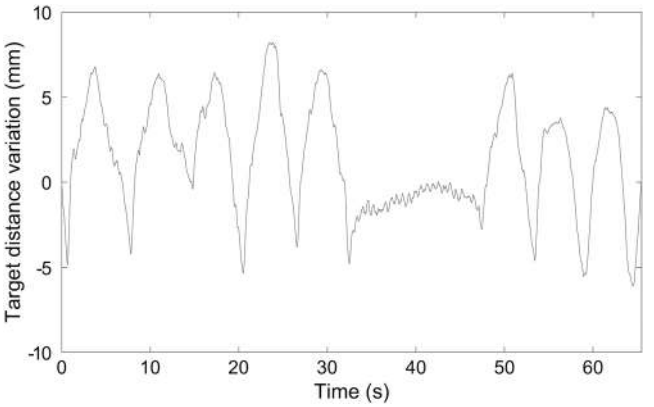


**Fig. 18** The breathing pattern curve.

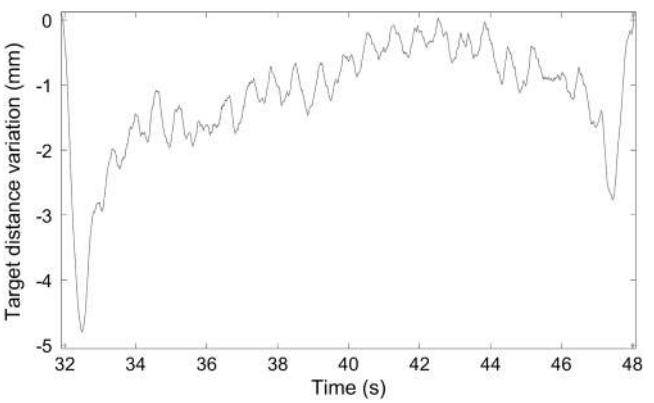


**Fig. 19** Heartbeat detected during the breath-holding section.

The second feasibility study was carried out outdoors in a heavy snowfall. The snowflakes were relatively large in size, the largest being >1 cm in diameter. The probing beam was directed at a target ~29 m away, and the laser beam was propagating through the falling snow. A TOF histogram including reflections from the target and also from individual snowflakes, at a distance of around 12 m, in addition to detections produced by the background illumination is presented in Fig. 20, whereas Fig. 21 shows a TOF histogram that provides a more accurate view of the detections caused by snowflakes at a distance of around 4.5 m. Individual snowflakes in both figures can be distinguished as separate

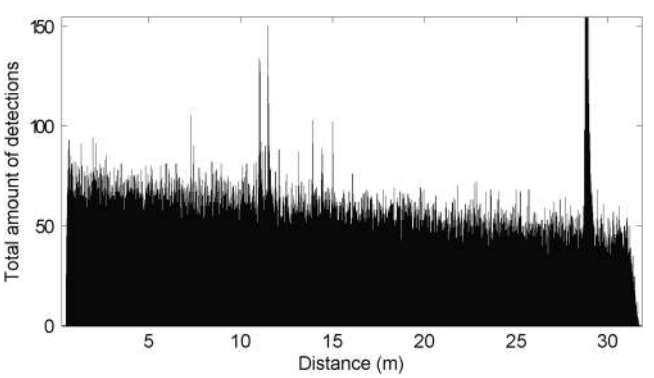


**Fig. 20** Snowflake detections at ~12 m.

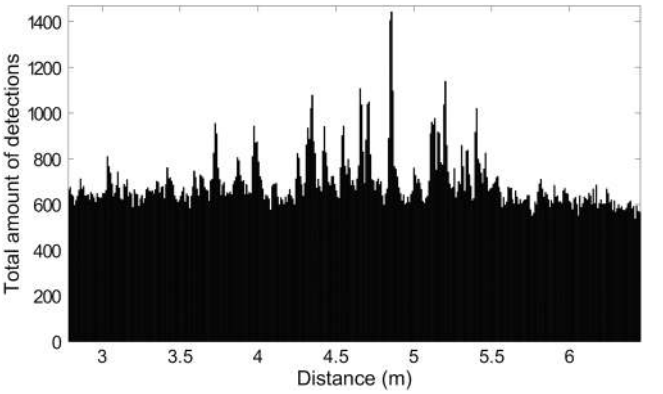


**Fig. 21** Snowflake detections at ~4.5 m.

spikes rising above the base level of the detections. The difference between the two histograms with respect to the distances at which snowflakes were detected is due to the different subarray selected in each case and the fact that the transmitter was focused at ~10 m. Note also the higher background noise level in Fig. 21, which is due to the longer measurement time. The experiment in question is an example of a measurement, which it is scarcely possible to perform with a conventional pulsed time-of-flight laser radar using a 3- to 5-ns laser pulse as a probe signal.

## 5 Discussion and Conclusions

A compact pulsed TOF laser radar module employing a CMOS SPAD array-based single-photon detection technique has been constructed and characterized. The key feature of the system from the miniaturization point of view is the transmitter, which uses a QW laser diode operating in the enhanced gain switching mode and driven by a relatively simple current pulsing scheme to produce high-power and high-speed laser pulses. The receiver is a single-chip CMOS IC including a $9 \times 9$ SPAD array detector and a 10-channel TDC circuit. The detector array ($9 \times 9$ SPAD elements) is configured to cover a substantially wider field of view (8.25 mrad) than that of the transmitter (0.75 mrad). This allows the receiver spot to move over the detector surface as a function of the measurement distance. The selectable $3 \times 3$ subarray feature allows spot tracking while simultaneously keeping the FOV of the detector, and thus the probability of detecting background photons is low. Since the amount of background power falling onto the detector is proportional to the second power of its field of view, every effort should be made at the system level to minimize the field of view of the SPAD detector. A larger overall detector area will also relax the requirements for mechanical tolerance in the optomechanics of the receiver. Finally, since the receiver spot energy inevitably falls on a larger number of SPAD elements due to defocusing, see Fig. 12, the TOF walk error at short distances, where the total signal strength is high, can be minimized by taking the TOF information from the SPAD element, which works in or near the single photon detection mode.

The laser diode and receiver IC are located on a single PCB at a distance of ~20 mm from each other, thus making the transmitter receiver module relatively compact. Yet, regardless of their close proximity, the photon detector electronics appear, due to their digital-like nature, to be immune

to the interference caused by the quite significant laser diode drive current pulse (~4 A, 1-ns FWHM).

The analysis and measurement results shown here demonstrate that the proposed current system enables a measurement range of several tens of meters to Lambertian targets with relatively high precision (mm level) and speed even under high background illumination conditions and with quite a compact realization. In particular, it has been shown that a large 2-D array as the detector is quite useful since it allows to achieve a small pixel size to be achieved with a large detector area. Thus, the background-induced detections can be minimized even though wandering of the received image spot on the detector surface is allowed. Moreover, if only SPAD elements working in the single photon detection mode are used, the walk error can also be minimized.

The laser radar architecture and design principles proposed here may well pave the way for the development of new simple and yet accurate miniaturized laser radars for a variety of applications.

## Acknowledgments

Academy of Finland (Centre of Excellence in Laser Scanning Research, Contract No. 272196 and Contracts Nos. 255359, 283075, and 251571); Finnish Funding Agency for Innovation (TEKES). The authors wish to express their gratitude to both the Academy of Finland and TEKES for supporting this work.

## References

1. M. Xuesong et al., "Amplitude-modulated laser radar for range and speed measurement in car applications," *IEEE Trans. Intell. Transp. Syst.* **13**(1), 408–413 (2012).
2. D. C. Carmer and L. M. Peterson, "Laser radar in robotics," *Proc. IEEE* **84**(2), 299–320 (1996).
3. J. Kostamovaara, K. Määttä, and R. Myllylä, "Pulsed time-of-flight laser range-finding techniques for industrial applications," *Proc. SPIE* **1614**, 283–295 (1991).
4. P. Palojärvi, K. Määttä, and J. Kostamovaara, "Pulsed time-of-flight laser radar module with mm-level accuracy using full custom receiver and TDC ASICs," *IEEE Trans. Instrum. Meas.* **51**(5), 1102–1108 (2002).
5. S. Donati, *Electro-Optical Instrumentation: Sensing and Measuring with Lasers*, Prentice-Hall, Upper Saddle River, New Jersey (2004).
6. S. Kurtti and J. Kostamovaara, "An integrated laser radar receiver channel utilizing a time-domain walk error compensation scheme," *IEEE Trans. Instrum. Meas.* **60**(1), 146–157 (2011).
7. J. Kostamovaara et al., "On laser ranging based on high speed/energy laser diode pulses and single photon detection techniques," *IEEE Photonics J.* **7**(2), 1–15 (2015).
8. C. Niclass et al., "Design and characterization of a 256×64-pixel single-photon imager in CMOS for a MEMS-based laser scanning time-of-flight sensor," *Opt. Express* **20**(11), 11863–11881 (2012).
9. A. Rochas et al., "Low-noise silicon avalanche photodiodes fabricated in conventional CMOS technologies," *IEEE Trans. Electron. Devices* **49**(3), 387–394 (2002).
10. M. Perenzoni, L. Pancheri, and D. Stoppa, "Compact SPAD-based pixel architectures for time-resolved image sensors," *Sensors* **16**(5), 745–756 (2016).
11. B. S. Ryvkin, E. A. Avrutin, and J. Kostamovaara, "Asymmetric-waveguide laser diode for high-power optical pulse generation by gain switching," *J. Lightwave Technol.* **27**(12), 2125–2131 (2009).
12. J. Huikari et al., "High-energy picosecond pulse generation by gain switching in asymmetric waveguide structure multiple quantum well lasers," *IEEE J. Sel. Top. Quantum Electron.* **21**(6), 189–194 (2015).
13. J. S. Massa et al., "Time-of-flight optical ranging system based on time-correlated single-photon counting," *Appl. Opt.* **37**(31), 7298–7304 (1998).
14. A. McCarthy et al., "Kilometer-range depth imaging at 1550 nm wavelength using an InGaAs/InP single-photon avalanche diode detector," *Opt. Express* **21**(19), 22098–22113 (2013).
15. M. Perenzoni, D. Perenzoni, and D. Stoppa, "A 64 × 64-pixels digital silicon photomultiplier direct TOF sensor with 100-MPhotons/s/pixel background rejection and imaging/altimeter mode with 0.14% precision up to 6 km for spacecraft navigation and landing," *IEEE J. Solid-State Circuits* **52**(1) 151–160 (2017).
16. V. Molebny et al., "Laser radar: historical prospective—from the east to the west," *Opt. Eng.* **56**(3), 031220 (2016).
17. M. A. Itzler et al., "Geiger-mode APD single-photon cameras for 3D laser radar imaging," in *Proc. of the 2014 IEEE Aerospace Conf.*, Big Sky, Montana, pp. 1–12 (2014).
18. J. Huikari et al., "A laser radar based on a 'impulse-like' laser diode transmitter and a 2D SPAD/TDC receiver," in *Proc. IEEE I2MTC Conf.*, Turin, Italy, pp. 927–932 (2017).
19. L. W. Hallman, J. Huikari, and J. Kostamovaara, "A high-speed/power laser transmitter for single photon imaging applications," in *Proc. of the IEEE Sensors Conf.*, Valencia, Spain, pp. 1157–1160 (2014).
20. S. Jahromi et al., "A single chip laser radar receiver with a 9×9 SPAD detector array and a 10-channel TDC," in *ESSCIRC 2015-41st*, Graz, Austria, pp. 364–367 (2015).
21. D. Bimberg et al., "Gain modulation of unbiased semiconductor lasers: ultrashort pulse generation," *Int. J. Electron.* **60**(23), 23–45 (1986).
22. P. Vasil'ev, *Ultrafast Diode Lasers: Fundamentals and Applications*, Artech House, Inc., Boston, London (1995).
23. J.-P. Jansson, A. Mantyniemi, and J. Kostamovaara, "A CMOS time-to-digital converter with better than 10 ps single-shot precision," *IEEE J. Solid-State Circuits* **41**(6), 1286–1296 (2006).
24. S. Jahromi, J. P. Jansson, and J. Kostamovaara, "Solid-state 3D imaging using a 1 nJ/100 ps laser diode transmitter and a single photon receiver matrix," *Opt. Express* **24**(19), 21619–21632 (2016).
25. J. Wang and J. Kostamovaara, "Radiometric analysis and simulation of signal power function in a short-range laser radar," *Appl. Opt.* **33**(18), 4069–4076 (1994).
26. G. Ramachandran and M. Singh, "Three-dimensional reconstruction of cardiac displacement patterns on the chest wall during the P, QRS and T-segments of the ECG by laser speckle interferometry," *Med. Biol. Eng. Comput.* **27**(5), 525–530 (1989).

**Jaakko Huikari** received his MSc Eng degree from the University of Oulu, Oulu, in 2014, where he has been working toward the PhD since. He was a research assistant in the University of Oulu between 2013 and 2014, doing a research on a single-photon detection-based laser radar. His current research interests include single-photon laser radar systems and laser transmitter and optical receiver development.

**Sahba Jahromi** received her MSc degree in electrical engineering-electronics from the University of Tehran, Tehran, Iran, in 2011. Since 2014, she has been working toward the Dr. Tech. degree in electronics at the University of Oulu, Oulu, Finland. Her research interests include single-photon detectors and circuits, pulsed time-of-flight techniques, and solid-state 3-D imagers.

**Jussi-Pekka Jansson** received his degrees of Dipl. Eng. and Dr. Tech in electrical engineering and title of adjunct professor in 2004, 2012, and 2017, respectively, all from the University of Oulu, Finland. He works as an Academy of Finland postdoctoral researcher at the same university, with the circuits and systems research unit. His research interests include high-precision time-to-digital converter architectures and applications related to them.

**Juha Kostamovaara** received his PhD in electrical engineering from the University of Oulu, Finland, in 1987. Currently, he holds a full professorship in electronics at the University of Oulu. His main research interests include the development of pulsed time-of-flight devices circuits, and systems for electronic and optoelectronic measurements.